Journal of Nano- and Electronic Physics
Vol. **9** No 6, 06008(5pp) (2017)

Журнал нано- та електронної фізики
Том **9** № 6, 06008(5cc) (2017)

Effects of Stone-Wales Defect Position in Graphene Nanoribbon Field-Effect Transistor

H. Owlia*, P. Keshavarzi†, M.B. Nasrollahnejad‡

Electrical and Computer Engineering Department, Semnan University, 3513119111 Semnan, Iran

(Received 25 July 2017; revised manuscript received 15 November 2017; published online 24 November 2017)

In this paper, the current-voltage characteristics of a double-gated monolayer armchair graphene nanoribbon field-effect transistor (DG-AGNRFET) is investigated by introducing a Stone-Wales (SW) defect. After changing positions of the defect in width and length of the channel, it is found that the SW defect decreases off current and leads to the further reduction of the off current as the defect moves to the edge. However, this defect has not shown a notable impact on the on current. The results have confirmed the possibility of controlling the electron transport of the DG-AGNRFET by defect engineering can be useful to extend the applications of graphene nanoribbon-based devices. The device has been simulated based on the self-consistent solution of a 3D Poisson-Schrödinger equation using non-equilibrium Green's function (NEGF) formalism.

Keywords: Device simulation, Graphene nanoribbon field-effect transistor (GNRFET), Non-equilibrium Green's function (NEGF), Stone-Wales defect.

DOI: 10.21272/jnep.9(6).06008

PACS numbers: 85.35. – p, 85.30.Tv, 68.65.Pq, 72.80.Vp, 73.22.Pr

1. INTRODUCTION

Defects in graphene caused by a crystalline disorder without the presence of foreign atoms like impurities are known as intrinsic defects and usually categorized based on different dimensionalities [1, 2]. We have four defect types namely zero, one, two and three dimensional intrinsic defects. The zero dimensional defects i.e. point defects are the most possible defects because of their low formation energies [1, 2]. Stone-Wales defect, vacancies, and adatoms are some of the conspicuous point defects commonly observed in monolayer and bilayer graphene [2-5].

A typical Stone-Wales (SW) defect involves an in-plain 90° rotation of a carbon-carbon bond in the honeycomb structure of a graphene sheet [6]. This process is accompanied with a structural relaxation until the change in total energy and forces on carbon atoms become less than 10^{-4} eV and 10^{-3} eV/Å respectively [7]. As matter of fact, it is found that such a dislocation experimentally can be created by irradiation, chemical treatments and during a rapid quench from high temperature [8-11].

Several studies have reported for the fundamental understanding of the electronic properties of the graphene including the SW defects. For example, Kvashnin et al. show that the effect of partial passivation on graphene nanoribbon (GNR) surface with a SW defect [7]. Zhao et al. present transport properties of a defected armchair GNR using spin-dependent calculations [12].

Up to now, there a few studies related to the *I-V* characteristics of the GNRFET including the SW defects. However, resent investigations are mainly devoted to phenomenological aspects of the defected GNR channel with small dimensions or GNRFETs with randomly distributed SW defects [7, 12-14]. So, this work intends to address the impact of the SW defect on *I-V* characteristics along and across the GNR channel in regular dimensions.

The rest part of the paper is organized as follows: Section 2 presents device configuration and computational methods applied in simulations. Section 3 shows simulation results for the presented structure. It is also shown that SW defects influence on carrier transport in the DG-AGNRFET. Finally, Section 4 expresses results and prospects.

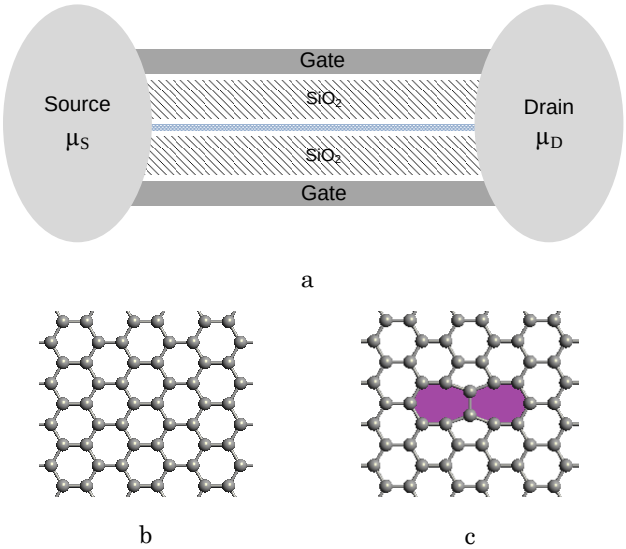

Fig. 1 – Simulated device structure (a), pristine graphene (b), a typical exploration of the SW defect (c)

2. APPROACH

The schematic diagram of the DG-AGNRFET is shown in Fig. 1a. A 10 nm long AGNR is used as a transistor channel and source/drain contacts include the doped n-type extensions of the AGNR channel. Two

* hadi.owlia@gmail.com
† pkeshavarzi@semnan.ac.ir
‡ mnasrollahnejad@semnan.ac.ir

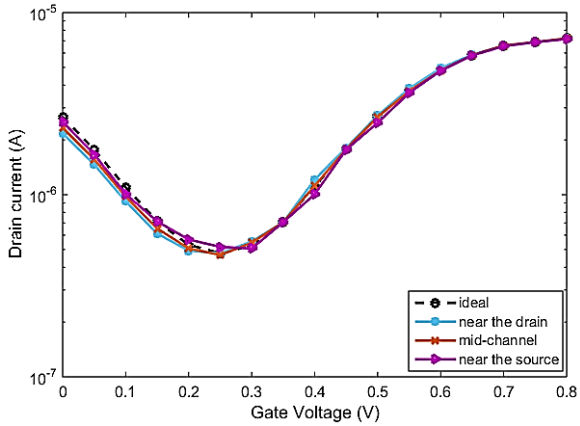

Fig. 2 – Drain current I_D versus gate voltage V_G characteristics for the DG-AGNRFET and defected DG-AGNRFET at different defect positions along the channel length when the drain bias V_D is 0.5 V

gate contacts are separated from nanoribbon by two oxide layers with a relative dielectric constant $3.9\varepsilon_0$ where ε_0 is the permittivity of vacuum. The oxides are made of SiO_2 and have 1.5 nm thicknesses. Stone-Wales (SW) defect consisting of a 90° in-plane rotation in each carbon-carbon bond is shown in Fig. 1b and 1c. In graphenic systems, the SW defect formation energetically is more favorable than that in carbon nanotubes and it has the lowest transformation energy among all intrinsic defects [15, 16]. The effects of SW defects in the both length and width directions of channel are studied in the simulated structure. Three different positions of the SW defects in the channel length and width are considered. These three positions in the channel length are 'near source', 'mid-channel' and 'near drain'. Also, three positions in the channel width are 'near edge', 'in-between' and 'center' and we consider the distribution of SW defects in the channel based on these positions.

All calculations required for quantum transport are performed using fully self-consistent tight binding model which is combined with non-equilibrium Green function formalism (NEGF) [17-21]. Advanced Green function of the channel between the source and drain regions can be calculated as follows:

$$G = \left[(E + i\eta) I - H_T - U - \Sigma_s - \Sigma_d\right]^{-1}, \qquad (2.1)$$

in which $\sum_s$ and $\sum_d$ are the self-energies describing the coupling between the device and source and drain regions, respectively. H_T is the tight-binding Hamiltonian matrix of the AGNR channel, which can be assessed with a tight-binding model [22]. U is self-consistent potential matrix and η is infinitesimally small quantity. Poisson equation simulates electrostatic potential distribution across the channel. Electrostatic potential U is obtained by solving the Poisson equation under Dirichlet boundary condition along the transport direction and Neumann boundary condition at the other boundaries. The Poisson equation is as follows:

$$\nabla^2 U = -\frac{q}{\varepsilon}\rho, \qquad (2.2)$$

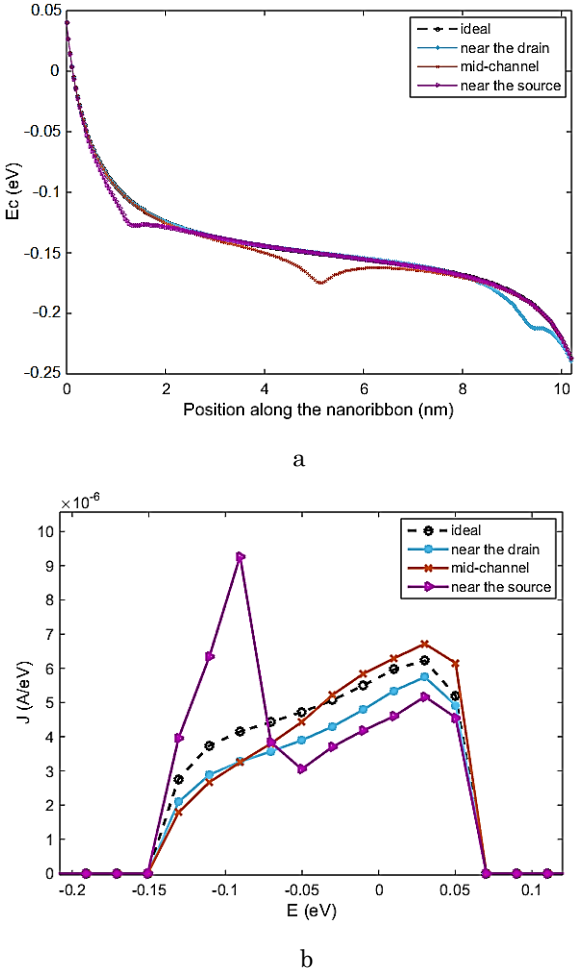

Fig. 3 – Conduction band profile E_c (eV) (a) and energy-resolved current spectrum J (A/eV) at the OFF state in three positions of the SW defect along the channel length (b) The reference energy level in the channel is set to be at the average of source and drain Fermi levels

where ε is dielectric constant and ρ is charge density. The charge density is determined by solving Schrödinger equation using the NEGF formalism.

Consequently, the transmission probability of carriers through the device can be written as:

$$T(E) = Trace\left[\Gamma_s G_D^r \Gamma_d G_D^a\right], \qquad (2.3)$$

where $\Gamma_{s/d} = i(\sum_{s/d} - \sum_{s/d}^{\dagger})$ is coupling between the contact of source/drain and device. $G^r{}_D$ and $G^a{}_D$ show advanced Green's function for the device region, which follows the relationship of $G^a = [G^r]^{\dagger}$ [23].

Electrical current is calculated through transmission spectrum and applying Landauer-Butiker equation [17]:

$$I = \frac{q}{h}\int T(E)\left[f(E-\mu_s) - f(E-\mu_d)\right]dE, \qquad (2.4)$$

where $T(E)$ is probability of passing of an electron with energy E through channel. q is electron charge, h is Planck constant and $f(E-\mu_{s(d)})$ is Fermi-Dirac distribution of carriers in contacts at chemical potential $\mu_{s(d)}$. All geometric nanostructures become relaxed so that

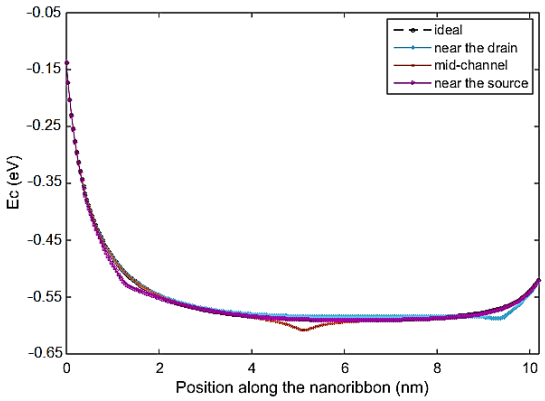

a

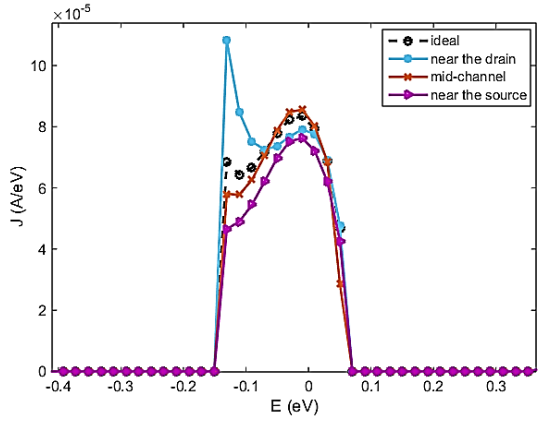

b

Fig. 4 – Conduction band profile E_c (eV) (a) and energy-resolved current spectrum J (A/eV) (b) at the ON state in three positions of the SW defect along the channel length; The reference energy level in the channel is set to be at the average of source and drain Fermi levels

atomic forces can't exceed 10^{-3} eV/Å and calculations are carried out at temperature $T = 300$ K.

3. RESULTS AND DISCUSSION

Fig. 2 shows the transfer characteristics of the DG-AGNRFET in the presence of the SW defects in three positions along the channel length. For a fair comparison, the minimum current of the ideal structure is selected to be off current where gate voltage approximately is 0.25 V and the ON state is calculated by adding supply voltage (here, $V_{DD} = 0.5$ V) to the OFF state. It is shown that the SW defect along the channel has no considerable effect on both the on and off currents. However, there is a little movement in the Dirac points of the curves in which electron and hole conductions are met.

The conduction band profile and energy-resolved current spectrum for all structures along the channel position are shown in Figs. 3 and 4. Although the transport window in the OFF state (from -0.15 to 0.07 eV) is located within variations of conduction band profile, the overall off current due to low current density has not shown remarkable changes. The transport window in the ON state is far from the edge of conduction band profile. So, the on currents remain the same in three defect positions.

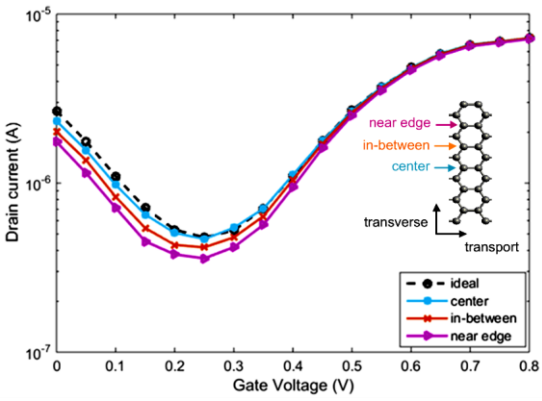

Fig. 5 – Drain current I_D versus gate voltage V_G characteristics for the DG-AGNRFET and defected DG-AGNRFET at different defect positions across the channel width when the drain bias V_D is 0.5 V

Fig. 5 shows the transfer characteristics of the DG-AGNRFET in the presence of the SW defects in three positions across the channel width. The SW defect decreases the off current and this reduction becomes more obvious as the defect moves to the edge although these defects have no impact on the on current (see Fig. 6 and 7).

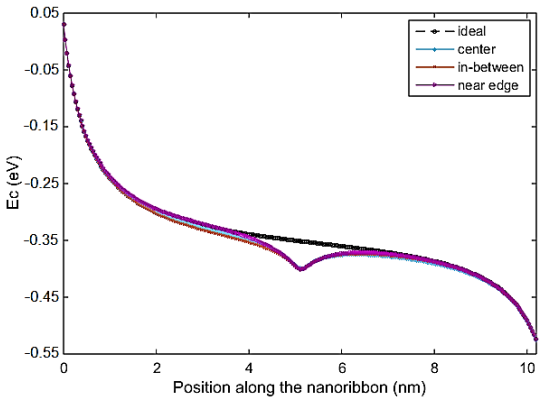

a

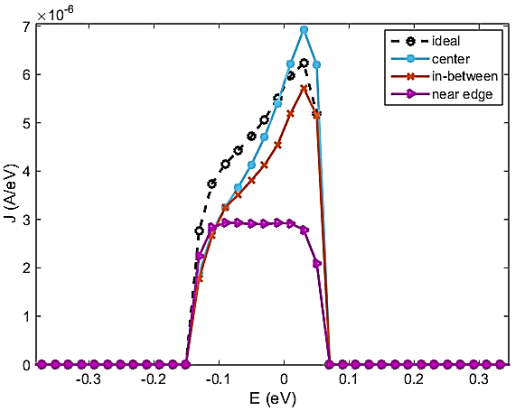

b

Fig. 6 – Conduction band profile E_c (eV) (a) and energy-resolved current spectrum J (A/eV) (b) at the OFF state in three positions of the SW defect across the channel width; The reference energy level in the channel is set to be at the average of source and drain Fermi levels

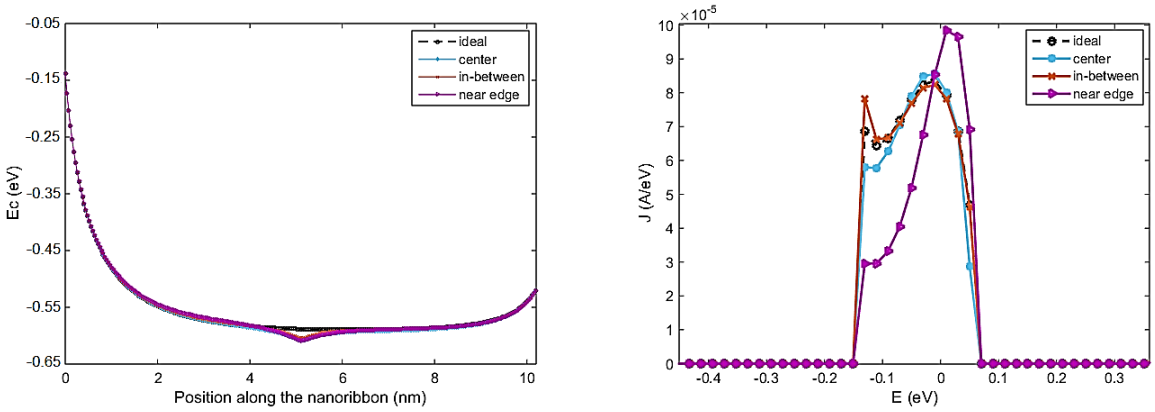

a b

Fig. 7 – Conduction band profile E_c (eV) (a) and energy-resolved current spectrum J (A/eV) (b) at the ON state in three positions of the SW defect across the channel width. The reference energy level in the channel is set to be at the average of source and drain Fermi levels

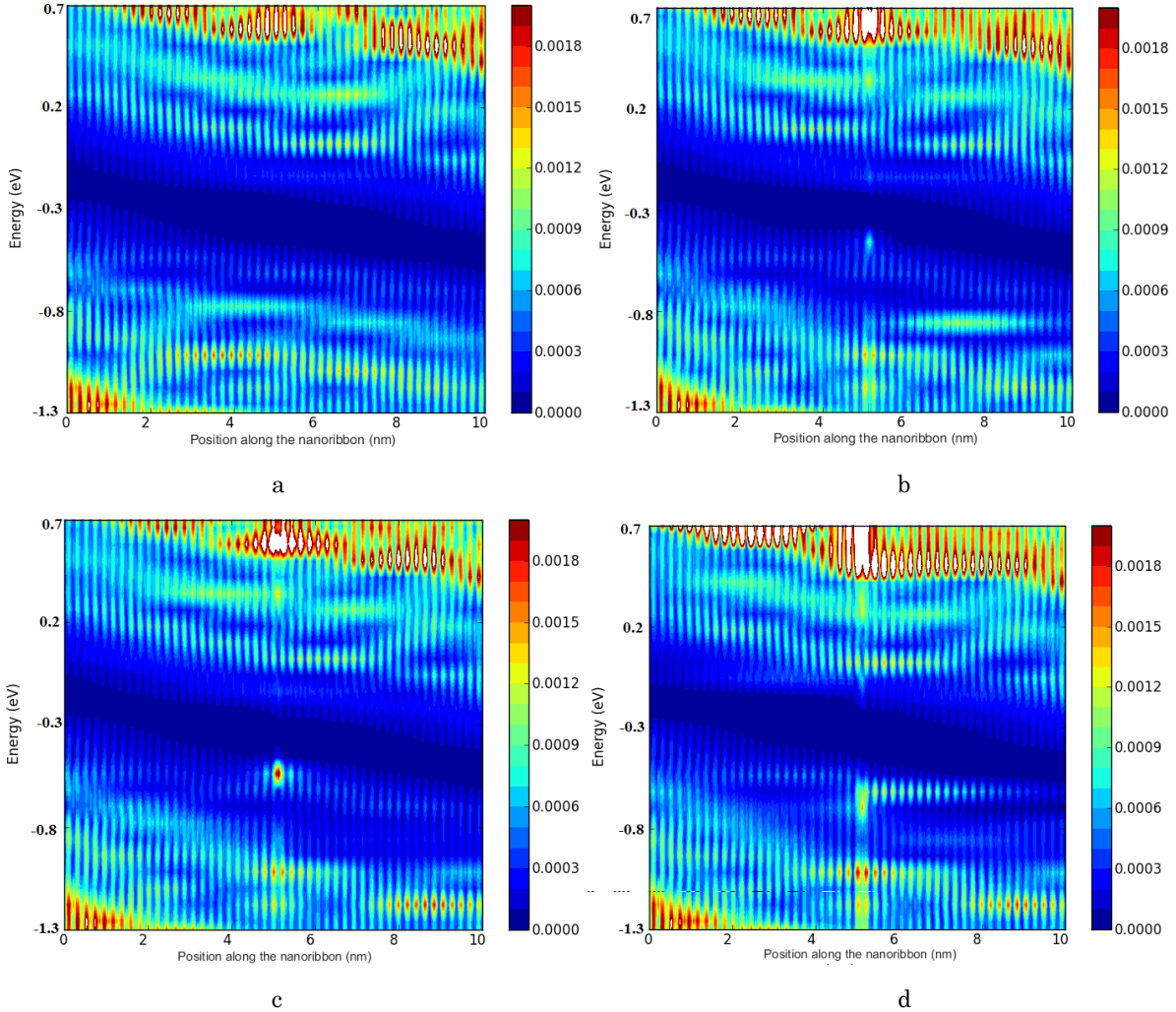

a b c d

Fig. 8 – LDOS at the OFF state for DG-AGNRFET (a) and defected DG-AGNRFET at different defect positions across the channel width (i.e. center (b) in-between (c) near edge (d)); In the white regions, the LDOSes are very high and those decrease as the regions become darker

In order to address the reason why the off current demonstrates noticeable reduction when the defect approaches the ribbon edge, the carrier transport behavior is assessed by local density of states (LDOS) profile. As shown in Fig. 8, the LDOS profile is illustrated for the ideal structure and the defected structures in three different positions across the channel width. In the vicinity of the edges of conduction and valance bands,

there are some localized states leading to electron-hole puddles in these regions. The brightness and area of the regions tends to be increasing as the defect moves to the ribbon edge. Generally, the results based on on-off current ratio can be summarized in Table 1. This value in the ideal structure is about 14.5. It is noted that the values in the table are normalized to that in the ideal DG-AGNRFET for indicating the percentage of improvements. As can be seen, the smallest and largest values are respectively devoted to the DG-AGNRFET with a SW defect near the source and the DG-AGNRFET with a SW defect near the edge. It would be expected that SW defects located at the positions near edge and drain-side of the channel are more favorable when the on-off ratio is being important.

Table 1 – On-off current ratio

DG-AGNRFET	Ideal	Near the drain	Mid-channel	Near the source	Center	In-between	Near edge
Real values	14.5	14.5	14.5	13.3	14.5	16.5	18.9
Normalized values	1	1	1	0.92	1	1.14	1.3

4. CONCLUSION

This paper evaluates a SW defect at different position along and across the channel. A SW defect is able to diminish off current and hence yields better on-off ratio. In the best case, defects close to drain are more promising. Additionally, there is partial movement of the Dirac point when the SW defects are located at different position along the channel. So, it can be found that gate engineering for tuning the OFF state can be obtained by choosing an appropriate position of SW defects rather than metal work function engineering.

REFERENCES

1. F. Banhart, J. Kotakoski, A.V. Krasheninnikov, *ACS Nano* **5**, 26 (2011).
2. L.D. Carr, M.T. Lusk, *Nat. Nanotechnol.* **5**, 316 (2010).
3. A.V. Savin, Y.S. Kivshar, *Phys. Rev. B* **88**, 125417 (2013).
4. A. Nazari, R. Faez, H. Shamloo, *Superlattice Microst.* **86**, 483 (2015).
5. A. Shokri, F. Khoeini, *Superlattice Microst.* **51**, 785 (2012).
6. K. Jin, H.Y. Xiao, Y. Zhang, W.J. Weber, *Appl. Phys. Lett.* **104**, 203106 (2014).
7. D.G. Kvashnin, L.A. Chernozatonskii, *Appl. Phys. Lett.* **105**, 083115 (2014).
8. L. Liu, M. Qing, Y. Wang, S. Chen, *J. Mater. Sci. Technol.* **31**, 599 (2015).
9. M. Anafcheh, R. Ghafouri, *Superlattice Microst.* **60**, 1 (2013).
10. J. Wang, G. Zhang, F. Ye, X. Wang, *J. Nanosci. Nanotechnol.* **16**, 8083 (2016).
11. M. Yamamoto, Y. Asayama, M. Yasuda, H. Kawata, Y. Hirai, *J. Vac. Sci. Technol. B* **32**, 06FK01 (2014).
12. J. Zhao, H. Zeng, B. Li, J. Wei, J. Liang, *J. Phys. Chem. Solids* **77**, 8 (2015).
13. H. Owlia, P. Keshavarzi, *IEEE T. Electron Dev.* **63**, 3769 (2016).
14. I.K. Petrushenko, *J. Nano- Electron. Phys.* **8**, 04052 (2016).
15. J.C. Meyer, C. Kisielowski, R. Erni, M.D. Rossell, M.F. Crommie, A. Zettl, *Nano Lett.* **8**, 3582 (2008).
16. J. Kotakoski, J.C. Meyer, S. Kurasch, D. Santos-Cottin, U. Kaiser, A.V. Krasheninnikov, *Phys. Rev. B* **83**, 245420 (2011).
17. S. Datta, *Quantum Transport: Atom to Transistor* (Cambridge: Cambridge University Press: 2005).
18. H. Owlia, P. Keshavarzi, *Superlattice Microst.* **75**, 613 (2014).
19. H. Owlia, P. Keshavarzi, *Mater. Sci. Semicond. Process.* **39**, 636 (2015).
20. M. Saremi, M. Saremi, H. Niazi, A.Y. Goharrizi, *Superlattice Microst.* **60**, 67 (2013).
21. Ali Naderi, *Superlattice Microst.* **89**, 170 (2016).
22. P.A. Alvi, S.Z. Hashmi, S. Dalela, F. Rahman, *J. Nano-Electron. Phys.* **3**, 42 (2011).
23. S. Datta, *Superlattice Microst.* **28**, 253 (2000).